Physical Science International Journal
11(3): 1-10, 2016, Article no.PSIJ.27566
ISSN: 2348-0130

SCIENCEDOMAIN *international*
www.sciencedomain.org

Chemical and Electrochemical Deposition of Ag onto Si for Fabrication of Si Nanowires and the Seebeck Effect Characterization

David Rodriguez[1] and Yong X. Gan[1*]

[1]Department of Mechanical Engineering, California State Polytechnic University, Pomona, 3801 W Temple Avenue, Pomona, CA 91768, USA.

Authors' contributions

This work was carried out in collaboration between both authors. Author DR performed the literature searches, did the experiments, collected the data and wrote the first draft of the manuscript. Author YXG designed the study and managed the experimental process. Both authors read and approved the final manuscript.

Article Information

DOI: 10.9734/PSIJ/2016/27566
Editor(s):
(1) Bheemappa Suresha, Department of ME, The National Institute of Engg, Mysore, India.
(2) Abbas Mohammed, Blekinge Institute of Technology, Sweden.
Reviewers:
(1) Androula Nassiopoulou, Institute of Nanoscience and Nanotechnology, Greece.
(2) Huang Xiaohu, Institute of Materials Research and Engineering, Technology and Research (A*STAR), 3 Research Link, Singapore.
(3) Wooyoung Lee, Yonsei University, Korea.
(4) Anonymous, India.
(5) Hao Wang, Technical center of China Tobacco Yunnan Industrial Co. Ltd, Yunnan, P.R. China.
Complete Peer review History: http://www.sciencedomain.org/review-history/15836

Original Research Article

Received 8th June 2016
Accepted 12th August 2016
Published 17th August 2016

ABSTRACT

In this work, vertically aligned porous Si nanowire (SiNW) arrays were successfully fabricated on two sides of an n-type Si wafer substrate. Ag nanoparticles (NPs) were first deposited onto the Si substrate via two different deposition methods, chemically and electrically (cyclic voltammetry), afterwards the metal assisted chemical etching (MaCE) technique was implemented to fabricate the SiNWs. The thermoelectric property of the SiNWs/Si/SiNWs structure was characterized by the Seebeck coefficient (S) which was measured at room temperature. Our results show a higher S when Ag NPs were electrodeposited onto the Si wafer piece compared to chemical deposition. The S enhancement is ~ 3 times and ~ 2 times in comparison to that of bulk Si and Ag chemical deposition samples, respectively. The electrodeposition created a strong adhesion between the Ag NPs and Si substrate which ensured a more uniform dispersed SiNWs producing a higher S. The

**Corresponding author: E-mail: yxgan@cpp.edu;*

improved thermoelectric performance coupled with electrodeposition of Ag indicates that the SiNWs/Si/SiNWs structure is an excellent candidate for the application in high-performance thermoelectric devices.

Keywords: Silicon; metal assisted chemical etching; silver deposition; thermoelectrics.

1. INTRODUCTION

Thermoelectric (TE) materials offer the opportunity for direct conversion of heat into electrical power for any temperature differences. This phenomenon plays a crucial role in solving today's energy problems such as energy shortage and pollution [1-4]. Furthermore, in medical applications, TE materials use body heat to generate power for devices such as biosensors and wearables [5-7]. The effectiveness of a TE material is best described in terms of a dimensionless TE figure of merit, $ZT = \frac{S^2\sigma T}{k}$ where $S = \frac{\Delta V}{\Delta T}, \sigma, T,$ and k are the Seebeck coefficient, the electrical conductivity, the absolute temperature, and the thermal conductivity, respectively [8]. A material with a very low k, a large S exposed to a small ΔT, and a large σ yields a maximum figure of merit. However, for a material to meet all these conditions simultaneously remains today's ongoing research challenge.

Semiconducting materials are often used as TE materials because of their high power factors ($S^2\sigma$) [9]. From all of the following researched semiconducting materials Si [9-14], Ge [15], Bi [7,15-17], SiGe [18], BiTe [18-20], and PbTe [21], Si remains the highest of research interest because of its nontoxicity, biocompatibility, good stability under high temperatures, abundant Si resource, and its interface compatibility with Si-based electronic devices [11,22]. Despite Si's high thermal conductivity ($k = 148\frac{W}{mK}$), it has been reported that rough silicon nanowires (SiNWs) have a high reduction in k compared to bulk Si [9,10,22]. It has too been reported that porosity on a nanomaterial can reduce the thermal conductivity [13]. A single SiNW [10] as well as an array of ≈ 100 SiNWs [14] have both reported a $ZT \approx 1$, making it a practical TE material [3]. There are two different approaches in fabricating SiNWs, the growth and etching approach. SiNWs that are typically obtained by the growth approach consists of assembling the nanowire, atoms at a time, through a mechanism called vapor-liquid-solid (VLS) using Au as a catalyze [23–26]. On the other hand, the etching approach consist of removing matter, atoms at a time, forming a nanowire. The etching approach has an advantage over growth because of its nanowire size (diameter and length) and its nanostructure organization at the surface of the silicon [27]. An example of an etching approach is the metal assisted chemical etching (MaCE) technique which is a popular fabrication technique because of its simplicity, low-cost, and its ability to control nonstructural parameters such as SiNWs' orientation, diameter, length, cross-sectional shape [27,28].

In this work, arrays of SiNWs were successfully synthesized by first depositing Ag nanoparticles (NPs) onto pieces of a n-type Si wafer via two different depositions, chemically and electrically. Secondly, implementing the MaCE technique to fabricate the SiNWs and creating an overall SiNWs/Si/SiNWs structure. The thermoelectric property of the fabricated SiNWs/Si/SiNWs structure was characterized by the Seebeck coefficient (S). This work investigated the S comparison of Ag chemical deposition verses electrodeposition and our results show a higher S outcome when Ag NPs are electrodeposited onto the Si substrate.

2. MATERIALS AND EXPERIMENTAL PROCEDURES

2.1 Preparation of SiNWs

The deposition of Ag NPs onto As-doped <100> n-type Si wafer pieces with the thickness of 500 micron and resistivity of 0.001~0.005 Ohm-cm was performed by two methods, chemical deposition and electrodeposition. Before the deposition of Ag, the five Si pieces used were cleaned in acetone and ethanol, followed by a 1 min pre-soak in a 4.8 M HF solution to remove any possible SiO_2 layers coated on the outside of the Si pieces. They were later rinsed with H_2O_2 followed by de-ionized water. Each piece was finally placed on a paper towel and left to air dry under room temperature. Chemical deposition of Ag onto the Si surface was performed on four of the five clean Si wafer pieces were chemically deposition with Ag by immersing the pieces in a solution of 0.01 M $AgNO_3$ and 4.8 M HF for 1 min. Afterward, three of the four Si pieces with

Ag NPs were MaCE in a 0.2 M H_2O_2 and 4.8 M HF solution, fabricating the SiNWs. After the three pieces were etched for 15, 30, and 60 mins, respectively they were removed and post-treated with de-ionized water to wash away any remaining residue.

On the last remaining clean Si piece, Ag NPs were electrodeposited via a cyclic voltammetry deposition for two cycles in a three-electrolytic cell. An Ag/AgCl (saturated KCl) electrode was used as both the reference and counter electrodes, and the Si piece as the working electrode. All potential in this study was measured with respect to the Ag/AgCl and both electrodes were submerged in a 0.6 M HNO_3 aqueous electrolyte solution. The working electrode was subjected to potential cycling from -5.0 to 1.0 V with an initial potential of 0 V at a rate of 10 mV s^{-1} until the second reduction sweep was achieved. This Si piece was next etched for 60 mins in a 0.2 M H_2O_2 and 4.8 M HF solution and post-treated with de-ionized water. After the completion of the MaCE process, each sample takes on a SiNWs/Si/SiNWs structure. All of the above procedures were performed under room temperature.

2.2 Characterization

The cyclic voltammetry deposition was carried out by connecting the three-electrolytic cell to a CHI 440C electrochemical workstation which measured and controlled the electrochemical parameters. The morphology of the SiNWs was observed using scanning electron microscope (SEM, Jeol JSM-6010PLUS/LA) with an accelerating voltage of 20.0 kV. The composition of the nanostructure was determined by energy dispersive X-ray spectroscopy (EDS). The S of the SiNWs/Si/SiNWs was measured at room temperature using an in-house built experimental apparatus consisting of a Talboys Basic Mini Aluminum Top Hot Plate, UEi INF 165 digital infrared thermometer, and the CHI 440C electrochemical workstation set to measure an open circuit voltage.

3. RESULTS AND DISCUSSION

3.1 Chemical Deposition

Fig. 1 illustrates the MaCE technique. In both chemical and electric depositions, the attached Ag^+ ions acquire electrons from the Si valence band and are reduced to form Ag NPs (nucleation). These NPs are soon injected into the Si creating oxidation (SiO or SiO_2) which is dissolved by HF. This continuous formation and dissolvent of SiO or SiO_2 underneath the Ag NPs allow the Ag NPs to sink inwards into the Si wafers (etching) forming tunnels and creating porous structures [28]. Due to the high density of Ag NPs, multiple tunnels could combine to form one wider tunnel [12]. The depth of these tunnels thus the length of the SiNWs increase approximately linearly with etching time [27,29]. As the Ag NP injects into the Si, it losses some of its ions (Ag^+) and diffusing into directions with low Ag^+ concentration. These Ag^+ ions can meanwhile be reduced to Ag NPs and/or Ag dendrites on the surface of the SiNWs. This loss of Ag^+ ions explanation is left out in Fig. 1.

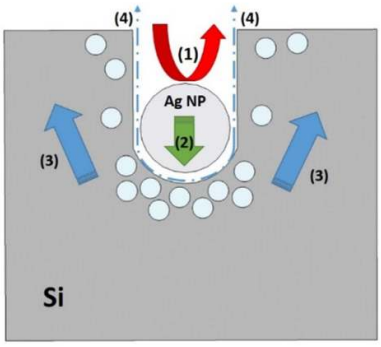

Fig. 1. The MaCE process: (1) the redox reaction of H_2O_2 and Ag; (2) the injection of the holes into the Si generated during the reduction, the highest hole concentration is located underneath the Ag NP; (3) the diffusion of holes to Si sidewalls and surfaces; and (4) the removal of oxidized Si by HF

3.2 Cyclic Voltammetry Deposition

Previous studies have shown that continuous cyclic voltammetry could produce more uniform and well-dispersed metal NPs with higher distribution density compared to metal NPs that were electrodeposited via constant potential [30]. Thus a cyclic voltammetry was used to deposit Ag NPs onto Si. The cyclic voltammogram (CV) of SiAg is presented in Fig. 2. The insert potential figure shows that a cycle starts with oxidation of Ag (-5 – 0 V) and ends with the redox of Ag^+ (0 – 1V). The arrows on the CV indicate the direction of the scan, and the blue and red lines are the 1st and 2nd cycle, respectively. There is a series of anodic events labeled A1 and A2 that were attributed to the oxidation of Ag. The explanation of the two consecutive oxidative peaks, A1 and A2, are attributed to hydroxides and Ag_2O, and remains a topic of ongoing research [31,30,32].

Peak A3 corresponds to the oxygen evolution. On the cathodic event, the current increases rapidly towards the C1 peak, indicating the redox couple of peaks A1 and A2, and the deposition of Ag^+ ions onto the Si piece. As described above, these Ag^+ nuclearize into Ag NPs on the surface of the Si substrate. The CV changes in currents between the two cycles are credited to the increase in surface roughness and in the number of the available nucleation and growth sites [33,34].

3.3 Morphology Characterization

The SEM images in Fig. 3 are the morphologies of the SiAg samples etched for 0 (a, SiAg), 15 (b, SiAg-15), 30 min (c, SiAg-30), and the energy dispersive x-ray diffraction spectrum of the sample SiAg-30 (d, SiAg-30 EDS). The SEM image of the SiAg-60 was also obtained (not shown here) from the sample with electrodeposited Ag NPs followed by 60 min etching. All SEM images were taken looking down onto the <100> plane of each sample. In Fig. 3a, the uniform distribution of Ag NPs is shown by the white dots. The darker shades of black shown in Fig. 3 b-c indicate porosity on the Si. This shows the formation of tunnels downward towards the Si substrate. The wider and longer shades of black illustrates the combination of multiple tunnels as described previously. Furthermore, the bright white dots are the tips of the SiNWs. To verify the chemical composition of the SiNWs/Si/SiNWs nanostructure, Fig. 3d is shown, which represents the results of the qualitative analysis of the elements using the EDS technique. This EDS figure confirms that Ag elements were attached to the Si surface before etching on all samples. All samples show similar counts of Ag to Si except for SiAg-30 which is due to the improper removal of Ag dendrites from the surface during post treatment and/or excess Ag^+ ions were present in the solution that were released by the SiAg-15 sample, since both were etched in the same solution in the same time.

The SEM image in Fig. 4(a) is the morphology of the sample that was etched for 60 mins after chemically depositing Ag NPs (SiAg*). The EDS results in Fig. 4(b) shows no Ag elements and confirms the oxidative nanostructure on the surface of the Si. This indicates the possibility that the Ag NPs did not fully bond onto the Si substrate causing the Ag NPs to deposit into the H_2O_2 and HF solution during the etching process. The 60 min etching time could cause the SiNWs to break off from the Si substrate dissolving into the etching solution. In view of the morphology formation mechanism, we believe that it is due to the oxidization of silicon. The Si loses electron and some of the Si dissolved into the solution. Therefore, some etching pits and plates shown in Fig. 4(a). That is the explanation of the facets formation in the SEM image. In Fig. 4(b), the EDS analysis of this sample is shown. The major element is Si. There are Al and C peaks, which is due to the signals from the sample holder and the conductive carbon tape. O peak is also observed. The EDS results confirm that no Ag is present due to the oxidization.

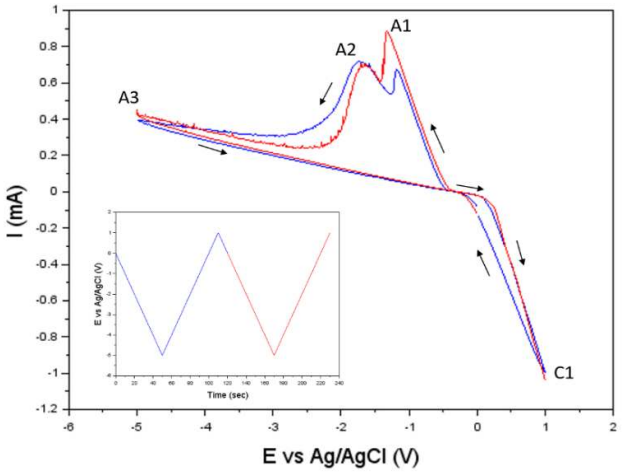

Fig. 2. Cyclic voltammogram of SiAg at a scan rate of 10 mV s^{-1} in a 0.6 M HNO_3 aqueous electrolyte solution. Insert shows the potential applied to the electrodes (blue and red indicate 1st and 2nd cycle, respectively)

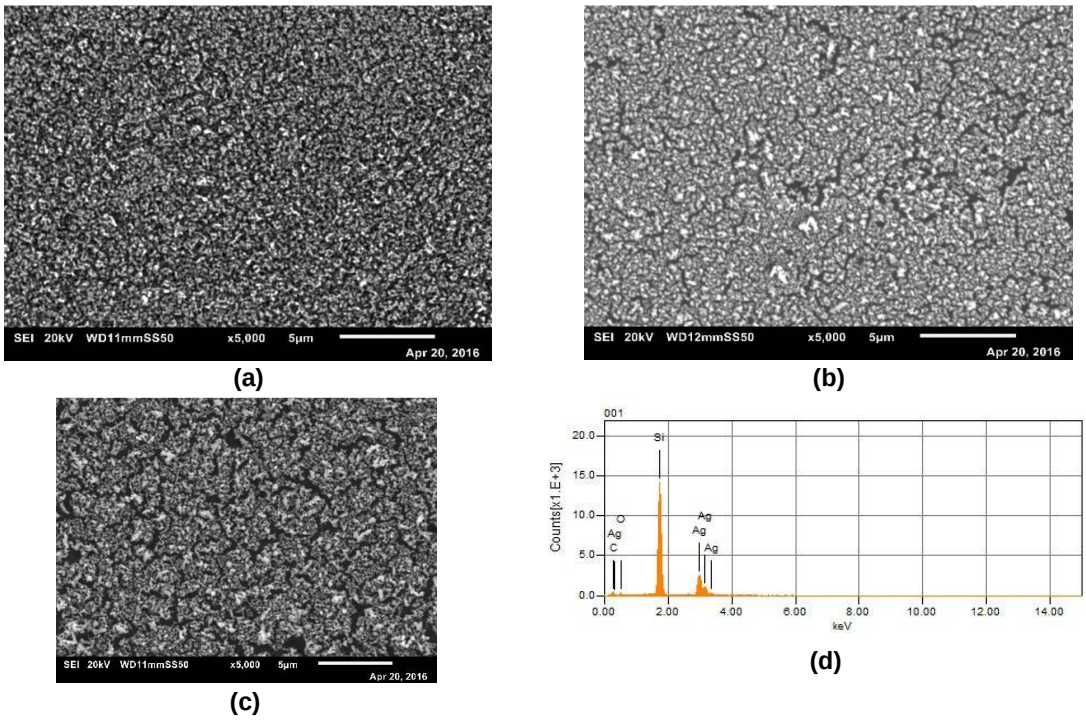

Fig. 3. Morphological SEM images from top-view, looking down onto the SiNWs, of (a) SiAg, (b) SiAg-15, (c) SiAg-30, and (d) EDS of SiAg-30

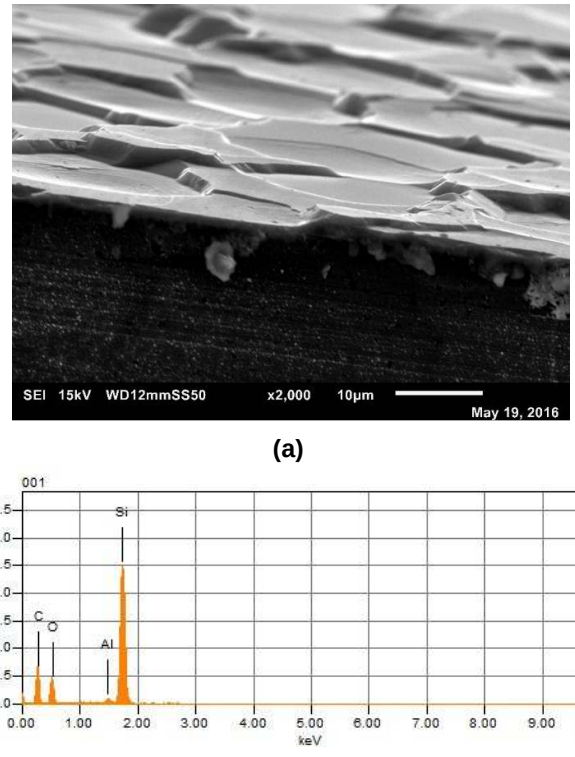

Fig. 4. (a) SEM image of SiAg* which shows the oxidation on the top of the Si substrate. (b) The EDS analysis of this sample confirms that no Ag is present due to the oxidization

3.4 Seebeck Coefficient Characterization

Fig. 5 shows a schematic diagram of our experimental apparatus. One end of the sample was sandwiched in between two aluminum cylinders and the other end was free-standing, similar to a cantilever. The bottom aluminum cylinder was heated using a hot plate and an insulator block was added underneath the free-standing section of the sample to prevent any heat convection from the hot plate. Using a digital infrared thermometer, temperature measurements were taken at the start (T_H) and end (T_C) of the cantilever (indicated by the red dots on Fig. 5), allowing measurement of temperature difference: $\Delta T = T_H - T_C$. This digital infrared thermometer measured the thermal radiation frequency distribution that each sample gave off, using this measurement it lastly calculates the temperature of the sample at an indicated point. Thus the temperature measured is a combination of both the bulk Si and top SiNWs array. When T_H remained constant, an open circuit voltage (ΔV) was measured as a function of time for 90 seconds. The Al foil served purposely as an electrode for measuring voltage. The voltage measurement error is 0.1 mV. The temperature measurement error is around 0.1 degree in Celsius.

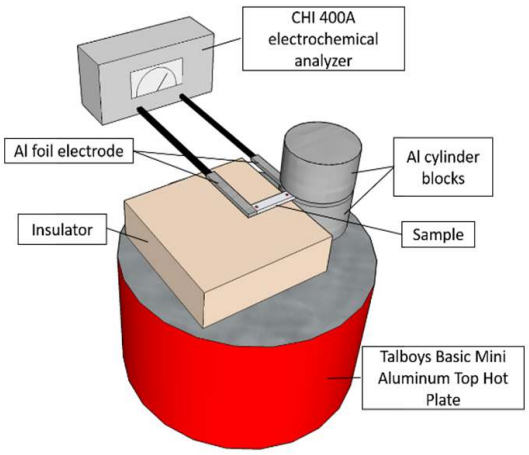

Fig. 5. A schematic diagram of our in-house built Seebeck coefficient measurement apparatus. The red dots on the sample indicates where the temperature measurement were taken

It is our intention to observing the Seebeck coefficient as a function of time. Therefore the time-dependent Seebeck coefficient changes are plotted. Fig. 6(a) shows S_{SiAg} with respect to time which has an average measurement of $0.09\frac{mV}{K}$ with a standard deviation of $0.04\frac{mV}{K}$. This result shows a 8-fold reduction in the S when a layer of Ag NPs, $S_{Ag} \approx 1.3\frac{\mu V}{K}$ [35], deposited onto the surface of bulk n-type Si, $S_{bulk} \approx 0.74\frac{mV}{K}$ [36], $S_{bulk} \approx 8\, S_{SiAg}$. $S_{SiAg-15}$ and $S_{SiAg-30}$ have an average measurement of $0.98\frac{mV}{K}$ (standard deviation of $0.02\frac{mV}{K}$) and $0.91\frac{mV}{K}$ (standard deviation of $0.05\frac{mV}{K}$), respectively as shown in Figure 6(b) and 6(c). It is documented that increasing etching time improves the thermoelectric properties [12], contradicting our $S_{SiAg-30}$ result. The significantly lower S_{Ag} compared to S_{Si} and the Ag to Si counts on SiAg-30 sample as discussed in the EDS studies above resulted in a 7% decrease from $S_{SiAg-15}$ to $S_{SiAg-30}$. Despite existing SiNWs, Ag dendrites and Ag^+ ions remained on the sidewalls and tips of the SiNWs causing the slight degeneration in S. Another possibility for the slight degradation has to deal with the Talboy's hot plate. The hot plate did not have the ability to keep its temperature stable, it functions by undergoing through heating and cooling cycles. Fig. 6c shows an example of the hot plate entering a cooling cycle indicated by the downward trend of $S_{SiAg-30}$. In addition, the S_{SiAg^*} was measured (average of $0.71\frac{mV}{K}$ and standard deviation of $0.02\frac{mV}{K}$) and resulted $0.03\frac{mV}{K}$ below S_{bulk} which validates the non-existent NWs.

Fig. 6(d) shows the measured $S_{SiAg-60}$ which resulted in a mean of $1.90\frac{mV}{K}$ and a standard deviation of $0.09\frac{mV}{K}$. There is a 3-fold improvement from S_{bulk}, $S_{SiAg-60} \approx 3\, S_{bulk}$ and a 2-fold improvement from SiAg-15 and SiAg-20, $S_{SiAg-60} \approx 2\, S_{SiAg-15} \approx 2\, Si_{SiAg-30}$. Table 1 shows the above S results. The improvement of electrodeposition from chemical deposition is associated with the adhesion of the nanoparticles (NPs) onto the Si substrate. In a previous study, it was found that Au, a noble metal like Ag, which was electrodeposited onto a Si substrate exhibits a much larger specific energy compare to a sputter deposition method [37]. Moreover, this same study found that the different behavior suggests that the mechanical interlocking between the Si and NPs contribute to a significant extent to the adhesion [37]. This same argument applies to this study. There existed a strong bond between the Ag NPs and the Si

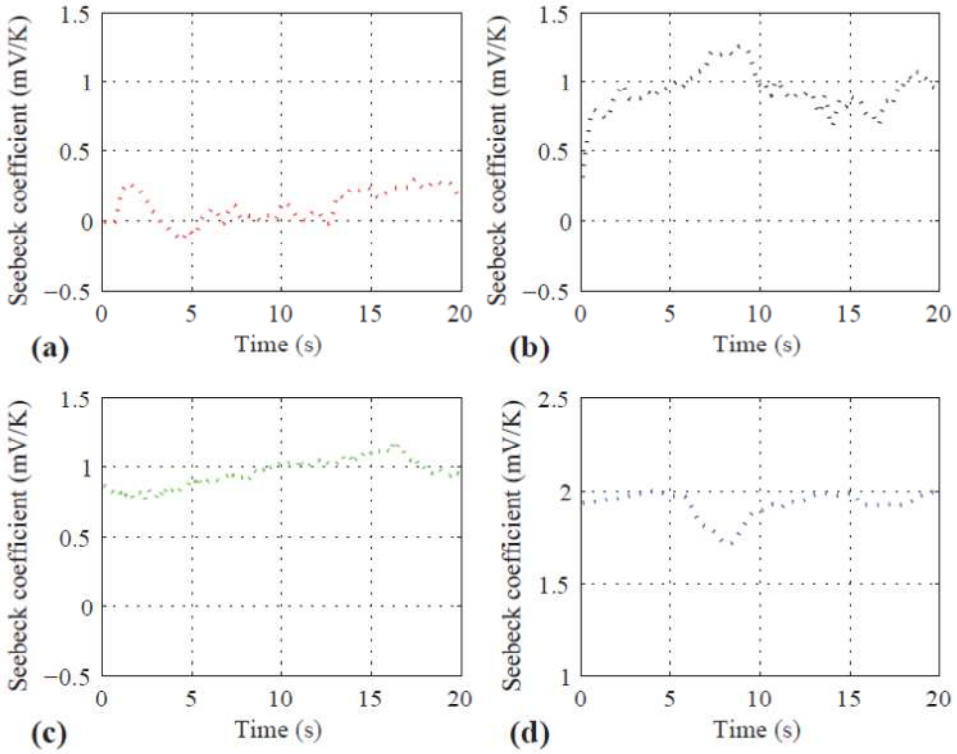

Fig. 6. Seebeck coefficient measuring results of (a) SiAg, (b) SiAg-15, (c) SiAg-30, and (d) SiAg-60

Table 1. Summary of measured thermoelectric property results

Sample	Ag deposit time	Etch. time	ΔT (K)	ΔV (mV)	S (mV/K)
SiAg	1 min	0 min	2.0	0.18	0.09
SiAg-15	1 min	15 min	2.0	1.95	0.98
SiAg-30	1 min	30 min	1.2	1.09	0.91
SiAg-30	Electro. (2 cycles)	30 min	1.2	1.61	1.33
SiAg-60	1 min	60 min	1.8	1.93	1.07
SiAg-60	Electro. (2 cycles)	60 min	1.8	3.37	1.90

substrate which ensured that the proper etching process was performed. As a result, SiAg-60 produced an array of nanowires that was more uniformly dispersed as compared with SiAg-15 and SiAg-30, resulting in a higher Seebeck coefficient value, S.

Harvesting thermal energy more effectively needs to control the properties of thermoelectric nanomaterials properly. Energy-related nanoscience and nanotechnology research has caught significant attention [38]. Here we compare the Seebeck coefficient of Si nanowires fabricated with the assistance of Ag nanoparticles with different approaches. One approach is the self-catalyzed chemical deposition. The other is the electrodeposition method. It is observed that Si nanowires synthesized with the assistance of electrically deposited Ag nanoparticles show higher Seebeck coefficient as discussed based on the results in Fig. 6. This point is meaningful for improving the thermal power of silicon nanomaterials. In order to further validate this, more comparative experiments are performed. Specifically, we would like to address one of the important issues on how to decouple the effect of etching time on the Seebeck coefficient. This allows us to make sure that the improvement on Seebeck coefficient due to the use of Ag particles made by electrodeposition method is significant. The following comparative experiment

results are presented in the last four rows of Table 1. The Seebeck coefficient value, S, of Si NWs fabricated by chemically deposited Ag NPs is compared with that of the sample using electrochemically deposited Ag NPs with the same etching time of 30 min. Si NWs fabricated by chemically deposited Ag NPs has the S value of 0.91 mV/K. While the Si NW sample using electrochemically deposited Ag NPs shows the S value of 1.33 mV/K. This is about 35% of increase. Similarly, Seebeck coefficient value of Si NWs fabricated by chemically deposited Ag NPs is compared with that of the sample using electrochemically deposited Ag NPs with the same etching time of 60 min. The Si NW sample using electrochemically deposited Ag NPs shows the S value as high as 1.90 mV/K. But the Si NWs fabricated by chemically deposited Ag NPs is much lower than this value. As shown in Table 1, the Seebeck coefficient of Si NW made using the chemically deposited Ag NPs is only equal to 1.07 mV/K. Again, this difference in the S values reveals the advantage of using the electrochemically deposited Ag NPs. Zhang et al. [12] found that the increasing in the etching time results in the slightly increasing in the S value. Our results as shown in both Fig. 6 and Table 1 are in agreement with their claim. However, the etching time effect seems not as significant as the use of electrochemically deposited Ag NPs.

4. CONCLUSION

SiNWs were successfully synthesized by first depositing Ag NPs by two methods, via chemical deposition and cyclic voltammetry deposition, onto a piece of n-type Si wafer and secondly implementing the MaCE technique. The S of the bulk SiNWs/Si/SiNWs were investigated and our results show a significant increase in S when Ag NPs are electrodeposited due to the strong bond between the Ag NPs and the Si substrate, $S_{SiAg-60} \approx 3\, S_{bulk}$. Moreover, research needs to be done to determine the S_{SiNWs} of samples similar to SiAg-60. Since $\Delta T = \Delta T_{SiNWs} + \Delta T_{Si}$, the values of ΔT_{SiNWs} and ΔT_{bulk} are determined only if the ratio of ΔT_{SiNWs}: ΔT_{bulk} was known. However, it is difficult to obtain these temperature differences experimentally or numerically because of the combination of heat conduction and convection, thus a finite element model will be ideal to approximate these values. Nevertheless, based on the results presented in this study, the thermoelectric performance improvement of the bulk SiNWs/Si/SiNWs, which are fabricated by using a combination of electrodeposition of Ag NPs and MaCE, is promising for the next generational thermoelectric devices.

ACKNOWLEDGEMENTS

This work is supported by the US National Science Foundation (NSF) under Grant Number CMMI-1333044. The SEM images were made possible through a NSF MRI grant DMR-1429674. The authors thank Professor Nicolas Fang at MIT for the useful discussion.

COMPETING INTERESTS

Authors have declared that no competing interests exist.

REFERENCES

1. DiSalvo F. Thermoelectric cooling and power generation. Science. 1999; 285(5428):703–706.
2. Bell LE. Cooling, heating, generating power and recovering waste heat with thermoelectric systems. Science. 2008; 321(September):1457–1461.
3. Snyder GJ, Toberer ES. Complex thermoelectric materials. Nat. Mater. 2008;7(2):105–114.
4. Wang YC, Dai CS, Wang SX. Theoretical analysis of a thermoelectric generator using exhaust gas of vehicles as heat source. Appl. Energy. 2013;112:1171–1180.
5. Olivo J, Carrara S, De Micheli G, De Micheli G. Energy harvesting and remote powering for implantable biosensors. IEEE Sens. J. 2011;11(7):1573–1586.
6. Bahk JH, Fang H, Yazawa K, Shakouri A. Flexible thermoelectric materials and device optimization for wearable energy harvesting. J. Mater. Chem. C. 2015;3: 10362–10374.
7. Leonov V, Gyselinckx B, Hoof C. Wearable self-powered wireless devices with thermoelectric energy scavengers. Integr. Issues Miniaturized Syst. - MOMS, MOEMS, ICS Electron. Components (SSI), 2008 2nd Eur. Conf. Exhib. 2008;1–8.
8. Dresselhaus MS, Lin YM, Rabin O, Dresselhaus G. Bismuth nanowires for thermoelectric applications. Microscale Thermophys. Eng. 2003;7(3):207–219.
9. Gonçalves AP, Lopes EB, Delaizir G, Godart C. Semiconducting glasses: A new class of thermoelectric materials? AIP Conf. Proc. 2012;1449:347–350.

10. Hochbaum AI, Chen R, Delgado RD, Liang W, Garnett EC, Najarian M, Majumdar A, Yang P. Enhanced thermoelectric performance of rough silicon nanowires. Nature. 2008;451(7175):163–167.
11. Li D, Wu Y, Kim P, Shi L, Yang P, Majumdar A. Thermal conductivity of individual silicon nanowires. Appl. Phys. Lett. 2003;83(14):2934–2936.
12. Zhang T, Wu S, Xu J, Zheng R, Cheng G. High thermoelectric figure-of-merits from large-area porous silicon nanowire arrays. Nano Energy. 2015;13:433–441.
13. Weisse JM, Marconnet AM, Kim DR, Rao PM, Panzer MA, Goodson KE, Zheng X. Thermal conductivity in porous silicon nanowire arrays. Nanoscale Res. Lett. 2012;7(1):3050-3016.
14. Boukai AI, Bunimovich Y, Tahir-Kheli J, Yu JK, Goddard WA, Heath JR. Silicon nanowires as efficient thermoelectric materials. Nature. 2008;451(7175):168–171.
15. Huang W, Koong CS, Liang G. Theoretical study on thermoelectric properties of Ge nanowires based on electronic band structures. Semicond. Semimetals. 2010;31(9):1026–1028.
16. Boukai A, Xu K, Heath JR. Size-dependent transport and thermoelectric properties of individual polycrystalline bismuth nanowires. Adv. Mater. 2006;18(7):864–869.
17. Heremans J, Thrush C. Thermoelectric power of bismuth nanowires. Phys. Rev. B. 1999;59(19):12579–12583.
18. Lee EK, Yin L, Lee Y, Lee JW, Lee SJ, Lee J, Cha SN, Whang D, Hwang GS, Hippalgaonkar K, Majumdar A, Yu C, Choi BL, Kim JM, Kim K. Large thermoelectric figure-of-merits from SiGe nanowires by simultaneously measuring electrical and thermal transport properties. Nano Lett. 2012;12(6):2918–2923.
19. Lee J, Kim J, Moon W, Berger A, Lee J. Enhanced seebeck coefficients of thermoelectric Bi 2Te 3 nanowires as a result of an optimized annealing process. J. Phys. Chem. C. 2012;116(36):19512–19516.
20. Gan YX, Koludrovich MJ, Zhang L. Thermoelectric effect of silicon nano fi bers capped with Bi – Te nanoparticles. Mater. Lett. 2013;111:126–129.
21. Pennelli G. Review of nanostructured devices for thermoelectric applications. Beilstein J. Nanotechnol. 2014;5(1):1268–1284.
22. Suh H, Jung H, Hangarter CM, Park H, Lee Y, Choa Y, Myung NV, Hong K. Diameter and composition modulated bismuth telluride nanowires by galvanic displacement reaction of segmented NiFe nanowires. Electrochim. Acta. 2012; 75:201–207.
23. Shi L. Thermal and thermoelectric transport in nanostructures and low-dimensional systems. Nanoscale Microscale Thermophys. Eng. 2012; 16(2):79–116.
24. Wagner RS, Ellis WC. Vapor-liquid-solid mechanism of single crystal growth. Appl. Phys. Lett. 2004;4(5):89-90.
25. Latu-Romain L, Mouchet C, Cayron C, Rouviere E, Simonato JP. Growth parameters and shape specific synthesis of silicon nanowires by the VLS method. J. Nanoparticle Res. 2008;10(8):1287–1291.
26. Redwing JM, Miao X, Li X. Vapor-liquid-solid growth of semiconductor nanowires. Handbook of Crystal Growth: Thin Films and Epitaxy: Second Edition. 2014;3:399–439.
27. Latu-Romain L, Ollivier M. Silicon carbide one-dimensional nanostructures (1). Wiley-ISTE. 2015;44–48.
28. Huang Z, Geyer N, Werner P, De Boor J, Gösele U. Metal-assisted chemical etching of silicon: A review. Adv. Mater. 2011;23(2):285–308.
29. Li X, Bohn PW. Metal-assisted chemical etching in HF/H_2O_2 produces porous silicon. Appl. Phys. Lett. 2000;77(16): 2572–2574.
30. Chen Y, Kirankumar R, Kao C, Chen P. Electrodeposited Ag, Au, and AuAg nanoparticles on graphene oxide-modi fi ed screen-printed carbon electrodes for the voltammetric determination of free sul fi de in alkaline solutions. Electrochimica Acta. 2016;205:124–131.
31. Cheng SL, Chung CH, Lee HC. A study of the synthesis, characterization, and kinetics of vertical silicon nanowire arrays on (001)Si substrates. J. Electrochem. Soc. 2008;155(001):D711.
32. Nagle LC, Ahern AJ, Burke LD. Some unusual features of the electrochemistry of silver in aqueous base. J. Solid State Electrochem. 2002;6(5):320–330.
33. Hur TU, Chung WS. The mechanism of silver(I) oxide to silver(II) oxide formation on polycrystalline silver electrodes in 8 M

KOH solution. J. Electrochem. Soc. 2005;152(5):A996–A1000.

34. Marenco AJ, Pedersen DB, Wang S, Petryk MWP, Kraatz HB. Electrochemical properties of gas-generated silver nanoparticles in the presence of cyano- and chloride-containing compounds. Analyst. 2009;134:2021–2027.
35. Cusack N, Kendall P. The absolute scale of thermoelectric power at high temperature. Proc. Phys. Soc. 1958;72(5): 898–901.
36. Krali E, Durrani ZAK. Seebeck coefficient in silicon nanowire arrays. Appl. Phys. Lett. 2013;102(14).
37. Zhu J, Henry P, Weaver ML, Reed ML, Zangari G. Enhanced adhesion of au films by electrodeposition onto porous Si. J. Electrochem. Soc. 2013;160(11):D507–D512.
38. Huang X, Xing G, Li Y, Nannen E. Nanomaterials for energy-efficient applications. J. Nanomater. 2015;2015: Article ID 524095:1-2.

Peer-review history:
The peer review history for this paper can be accessed here:
http://sciencedomain.org/review-history/15836